Kinematics of the Doped Quantum Vortices in Superfluid Helium Droplets

Charles Bernando[1] and Andrey F. Vilesov[1,2,a)]

[1] Department of Physics and Astronomy, University of Southern California, Los Angeles, California 90089, USA
[2] Department of Chemistry, University of Southern California, Los Angeles, California 90089, USA

[a)]Author to whom correspondence should be addressed. Electronic address: vilesov@usc.edu.

January 9, 2018

Abstract

Recent observation of quantum vortices in superfluid ^{4}He droplets measuring a few hundreds of nanometers in diameter involved decoration of vortex cores by clusters containing large numbers of Xe atoms, which served as x-ray contrast agents. Here, we report on the study of the kinematics of the combined vortex-cluster system in a cylinder and in a sphere. Equilibrium states, characterized by total angular momentum, L, were found by minimizing the total energy, E, which sums from the kinetic energy of the liquid due to the vortex and due to orbiting Xe clusters, as well as solvation energy of the cluster in the droplet. Calculations show that, at small mass of the cluster, the equilibrium displacement of the system from the rotation axis is close to that for the bare vortex. However, upon decrease of L beyond certain critical value, which is larger for heavier clusters, the displacement bifurcates towards the surface region, where the motion of the system is governed by the clusters. In addition, at even smaller L, bare orbiting clusters become energetically favorable, opening the possibility for the vortex to detach from the cluster and to annihilate at the droplet's surface.

1. Introduction

Quantum vortices are one of the most spectacular manifestations of superfluidity [1-3]. In contrast to a normal fluid, which in equilibrium rotates as a rigid body, a superfluid remains at rest when its container has low angular velocity. However, above a certain critical angular velocity the thermodynamically stable state of a superfluid includes one or more quantum vortices. In equilibrium, quantum vortices assume some symmetric configurations, which are stationary in the frame rotating with constant angular velocity. Experimental study of quantum vorticity hinges on the observation of the vortex cores. Quantum vortices in rarified trapped Bose-Einstein condensates (BECs) have been extensively studied over the past two decades. [3-7] Vortices in BEC can be observed via optical microscopy, due to large diameter of a core containing region of small density ~1 μm, which are then further magnified upon the condensate expansion. In contrast, the vortices in superfluid ^{4}He have very small core diameter of the order of ~0.2 nm and their observation usually involves tracing particles trapped in cores by hydrodynamic forces. The vortices in ^{4}He were first visualized using electrons.[8-10] Tracing with micrometer-sized hydrogen clusters was used to study the dynamics of the vortex filaments on the sub millimeter length scale, such as vortex reconnection and Kelvin waves [11-14]. He_2* excimer molecules are also promising tracers, which can easily be produced via electron impact or upon irradiation by focused femtosecond laser pulses and detected by laser induced fluorescence [11, 15-17]. However, no tracing of single vortex filaments with He_2* has been demonstrated thus far.

Free superfluid helium droplets have been long considered as an ideal system for quantum hydrodynamics studies. Early attempts at observing vortices in millimeter-sized He droplets include experiments with magnetic levitation [18, 19]. Even smaller micron and nanometer sized droplets could be produced in a free jet expansion [20-23], which breaks into rotating droplets [24-26]. Quantum vortices were visualized via x-ray coherent diffractive imaging upon doping of the

droplets with Xe tracers [24, 26-28]. The analysis of the diffraction images [28] shows that doped vortices in the droplets with radius of $R_{He} \sim 100$ nm form symmetric configurations with relatively large distance from the droplet center ($r \approx 0.7\ R_{He} - 0.8\ R_{He}$).

Theoretical interest in configurations of vortices in finite systems dates to Lord Kelvin [29]. The shapes and dynamics of bare vortices in a container with fixed boundary conditions can be calculated using the Biot-Savart law [30-33]. However, the implementation of this approach, which requires calculation of the vortex images, is only feasible for simple geometries, such as in a square channel, in a cylinder or in a sphere [30-33]. The expansion of this approach to systems with free deformable surface, such as in a droplet or for doped vortices has not yet been demonstrated. Very recently, the positions of a few vortices in droplets with $R_{He} \sim 5$ nm were obtained via density functional calculations [34]. For bare vortices in a cylinder experiments [9] and calculations [35, 36] as well as calculations in the droplets [34] indicated that at large distance from the center of $r > 0.7\ R$ vortex formations are unstable with respect to vortex annihilation at the surface. Time dependent density functional TDDFT calculations in small He droplets containing 15000 atoms confirmed that doped vortices with large displacement are stable at values of the angular momentum well below the stability limit of an undoped droplet [37]. In addition, capture of atoms by a quantum vortex has recently been studied theoretically in bulk LHe [38] and in He droplets [37]. Kinematics of the doped vortices have also been studied by solving generalized nonlinear Schrodinger equations [39]. Experimental observation of vortices with large displacement from the center of the droplet [28] indicates that the presence of the tracers in the vortex cores critically influences the kinematics of the system, which is the focus of this paper. Here, we present the results of the model for equilibrium positions of single doped vortices in a free cylinder and in a sphere with fixed angular momentum. The calculations are based on previous

studies of the configurations of bare vortices [40, 41] in the droplets which were modified in order to include the kinetic energy and angular momentum of the trapped clusters. An additional potential energy term arises due to solvation energy of the dopants in liquid helium. As a result, there exist equilibrium positions of single doped vortices close to the surface of the droplets.

2. Vortex in a free droplet

In equilibrium, the doped vortices are stationary in a frame rotating with some angular velocity, ω, with respect to the laboratory frame. Therefore, Xe clusters contribute to the total kinetic energy and angular momentum of the system. The equilibrium configuration of a doped vortex in a free droplet with total angular momentum L is determined by minimizing the total energy E:

$$L = L_{vort} + L_{clust} \tag{1}$$

$$E = E_{vort} + E_{clust} + V_{solv} \tag{2}$$

where L_{vort} (E_{vort}) and L_{clust} (E_{clust}) are the angular momenta (kinetic energies) due to vortex and cluster revolving with the vortex. V_{solv} is the solvation energy of the cluster in the He droplet. In the case when a vortex and axis of rotation lay in the same plane, the L_{vort} and E_{vort} can be expressed as [40]:

$$E_{vort} = \frac{1}{2}\rho_S \kappa \int \vec{v}_S \cdot d\vec{S} \tag{3}$$

$$L_{vort} = \rho_S \kappa \int \vec{d} \times d\vec{S} \tag{4}$$

where ρ_S is the superfluid density, is v_S is the superfluid velocity due to vortex and d is the vector distance of each vortex element from the center of a cylinder or a sphere. The quantum of circulation $\kappa = h/M$, where h is the Planck's constant and M is the mass of ^{4}He atoms. The area of

integration, dS, is the region circumscribed by the vortex and the drop surface in the plane of the vortex. Note that in case of a droplet rotating with a fixed angular velocity, such as in a rotating bucket experiment, the equilibrium is described by minimization of its free energy F in the rotating frame [1, 3, 40]:

$$F = E - L \cdot \omega \quad . \tag{5}$$

In this paper, we neglect any contribution from the backflow due to different local velocity of the cluster and its liquid environment, which seems to be a good approximation as the density of solid Xe is a factor of ~26 larger than of liquid helium. In addition, we neglect contributions to L and E from the normal component of liquid helium. At relevant $T = 0.4$ K, the effective moment of inertia due to phonons is 1.7×10^{-6}, whereas that arising from riplons is $\sim1.4\times10^{-4}$ (R_{He} = 100 nm) in the units of the classical moment of inertia in a spherical droplet [26, 42] The contributions due to phonons and riplons scale as T^4 and $T^{5/3}/R_{He}$, respectively. Thus, at typical experimental conditions, the moment of inertia due to Xe clusters is a factor of ~100 larger than that due to phonons and riplons. Nevertheless, the presence of the thermal excitations of the normal component assure that upon equilibration, the doped vortex and the normal component are stationary in the frame rotating with some angular velocity ω. We have also assumed rotation around the center of the cylinder/sphere, neglecting any center of mass effects in the doped droplets. Centrifugal deformation of the droplets is also neglected. Finally, throughout the calculations, we have assumed that the vortex is pinned to the Xe filament in its core along the entire length. Section 6 will present a discussion of possible dissociation events.

3. Solvation Potential for Xe Clusters in Liquid Helium

Solvation potential, V_{solv}, results from the van der Waals interaction of the atoms in the embedded cluster with the He atoms of the droplet. In the close proximity (< 1 nm) of the cluster, the He density is enhanced [43, 44]. However, away from the cluster, the droplet has a constant density and the interaction between the atoms in the cluster and the He atoms in the liquid is represented by the long range attractive potential [45]:

$$V(s) = -\frac{C_6}{s^6} \tag{6}$$

where s is the distance between the interacting atoms and C_6 is the dispersion interaction constant, which is 0.23 K·nm^6 [46] for He and Xe. V_{solv} is then approximated as a sum of the pair wise interactions between the Xe atoms in the cluster and He atoms of the droplet. To simplify the integration, we have discretized the clusters and He liquid with the smallest unit defined as a 1 nm^3 cube. Figure 1 shows the calculated solvation potentials per 1 nm length of cylindrical Xe-filaments of solid density with radii of R_{Xe} = 2.5, 5, and 10 nm in a He cylinder with R_{He} = 100 nm versus the distance from the center, r. It is seen that the solvation potential is flat in the inner part and increases sharply in the surface region at r > 80 nm. Thus, the solvation potential prevents the filaments and the pinned vortices from a close approach to the surface.

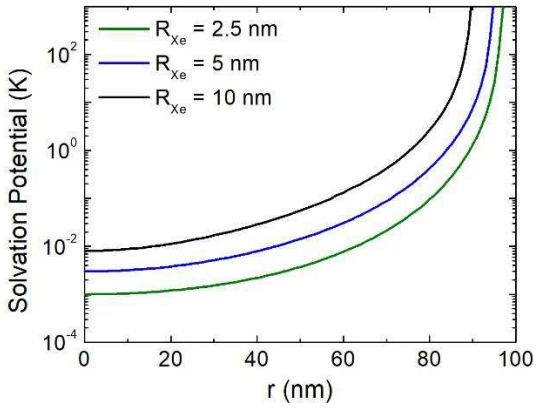

Figure 1. Solvation potential per 1 nm length in K units for solid Xe filaments, having a radius of R_{Xe} = 2.5, 5, and 10 nm (from bottom to top) in a free cylinder of liquid He, having a radius of R_{He} = 100 nm. The plots are shifted upwards by 10^{-3}, $3\cdot10^{-3}$ and $9\cdot10^{-3}$ K, respectively, to avoid the cusp at r=0.

4. Doped Rectilinear Vortex in a Cylinder

Vortices in a cylinder filled with a superfluid present the simplest possible model system that can be treated via analytic equations [35]. Accordingly, in the case of a doped rectilinear vortex in a cylinder, equations (1,2) (per unit length) can be expressed as:

$$E = \frac{\rho_{He}\cdot\kappa^2}{4\cdot\pi}\cdot\ln\left(\frac{{R_{He}}^2 - r^2}{R_{He}\cdot\xi}\right) + \frac{\rho_{Xe}\cdot\pi\cdot{R_{Xe}}^2\cdot\left(0.5\cdot{R_{Xe}}^2 + r^2\right)\cdot\omega^2}{2} + V(r) \tag{7}$$

$$L = \frac{1}{2}\cdot\rho_{He}\cdot\kappa\cdot\left({R_{He}}^2 - r^2 - \xi^2\right) + \rho_{Xe}\cdot\pi\cdot{R_{Xe}}^2\cdot\left(0.5\cdot{R_{Xe}}^2 + r^2\right)\cdot\omega \tag{8}$$

where r is the distance of the filament from the cylinder axis, ρ_{He} = 145 kg/m^3 is the density of liquid helium, ρ_{Xe} = 3781 kg/m^3 is the density of solid Xe, R_{He} is the radius of the cylinder, κ = 9.97×10^{-8} m^2/s is the quantum circulation, ξ is the radius of a vortex core. The parameter ξ assumes a value of 10^{-10} m in a bare vortex, whereas with Xe filament it is approximated by R_{Xe}.

In case of a bare vortex the solutions are [35]:

$$E = \frac{\rho_{He} \cdot \kappa^2}{4 \cdot \pi} \cdot \ln\left(\frac{R_{He}^2 - r^2}{R_{He} \cdot \xi}\right)$$

$$L = \frac{1}{2} \cdot \rho_{He} \cdot \kappa \cdot \left(R_{He}^2 - r^2 - \xi^2\right)$$

$$\omega = \frac{dE}{dL} = \frac{\kappa}{2 \cdot \pi \cdot \left(R_{He}^2 - r^2\right)}$$

$$r = \sqrt{R_{He}^2 - \xi^2 - \frac{2L}{\rho_{He} \cdot \kappa}} \qquad (9)$$

It is seen that r, E, and ω can be expressed in terms of the total angular momentum L. In the following, we present the results in terms of the reduced values of r, L, E, and ω defined as: $r_r = \frac{r}{R}$, $L_r = \frac{L}{L(0)}$, $E_r = \frac{E}{E(0)}$ and $\omega_r = \frac{\omega}{\omega(0)}$, where $L(0)$, $E(0)$ and $\omega(0)$ are corresponding values for a rectilinear vortex at the center of the cylinder ($r = 0$). In calculating the reduced values in the presence of Xe, ξ values were taken to be equal to the radius of the Xe filament. For a bare vortex in a cylinder of R_{He} = 100 nm: $L(0) = 7.2\times10^5$ ħ/nm, $E(0)$ = 57 K/nm and $\omega(0) = 1.6\times10^6$ rad/s. Equations (7,8) give the equilibrium distance r which minimizes energy in eq. (7) for a given L. Fig. 2 shows the calculated values for r_r, E_r and ω_r versus L_r.

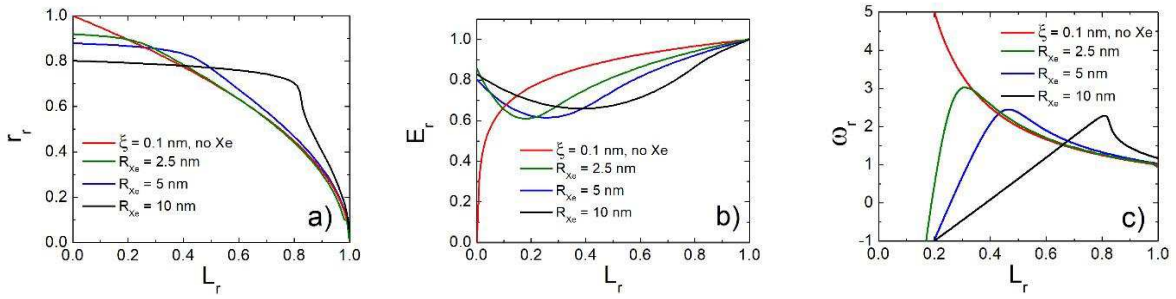

Fig. 2. Plots of (a) reduced equilibrium position r_r, (b) reduced energy E_r, and (c) reduced angular velocity ω_r as a function of reduced angular momentum L_r for a system of quantum vortex in a cylinder with R = 100 nm without (red curve) and with Xe filament with radii of R_{Xe} = 2.5 nm, 5 nm, and 10 nm, shown by green, blue, and black solid curves, respectively.

Fig. 2 a) shows that, with decrease in total angular momentum, the bare vortex moves away from the center, until it reaches the surface of the cylinder before getting annihilated at $L = 0$. In the doped vortex the energy and the angular momentum are partitioned between the vortex and the Xe filament according to Eqs. (7,8). Upon increase of the mass and radius of the filament the kinetics changes from that dominated by the vortex to that dominated by the filament. It is seen that the presence of a Xe filament leads to an increase of r_r that can be ascribed to a centrifugal force on the vortex. In addition, doped vortices cannot come too close to the surface due to the solvation potential, leading to a maximum of $r_r \approx 0.8\text{-}0.9$ that persists even as L_r approaches zero. Fig. 2 b) shows that the energy of the bare vortex decreases monotonically, as L_r decreases from 1 to 0. The total energy of the system with Xe filament remains very close to that for the bare vortex with $\xi = R_{Xe}$ in the range of $L_r = 1 - 0.3$. However, at smaller L_r , E_r stagnates reaching a minimum at $r_r \sim 0.2\text{-}0.4$ and starts increasing at smaller L_r . Lastly, Fig. 2 c) shows the L_r dependence of the reduced angular velocity ω_r. The ω_r values for the bare and doped vortices are very similar until the doped vortex reaches the surface region, where its motion is substantially influenced by the solvation potential. In the surface region, the angular velocity of a bare vortex increases rapidly. For the bare vortex, the velocity of the vortex core is determined by the local velocity field of the image vortex, which position becomes closer to the surface at large r_r. The image vortex no longer defines the ω_r of the doped droplets. In the surface region, ω_r of the doped vortex decreases and even becomes negative at small L_r. As the L_{vort} remains approximately constant in the surface region, the total L can only be reduced by a decrease in ω, and eventually reversing the sense of rotation. Solutions with negative ω_r are metastable, whereas the stable solution corresponds to a revolving filament without a vortex as it will be discussed in Section 6 for a vortex in a sphere. Although the calculations in Fig. 2 were done with the potentials in Fig. 1, very similar results

could be obtained using a box potential, in which the potential is zero inward and rises to infinity at some distance from the surface.

Finally, we note that the results displayed in Fig. 2 could be obtained from the equilibrium of forces acting on the doped vortex, which include the centrifugal force, the force due to solvation potential and the Magnus force, dwelling from the difference of the local velocity of the superfluid as determined by the image vortex, v_s, and velocity of the doped vortex, $\omega \cdot r$.

$$F = \rho_{Xe} \cdot \pi \cdot r_{Xe}{}^2 \cdot \omega^2 \cdot r - \frac{dV}{dr} + \kappa \cdot \rho_{He} \cdot \left(\frac{\kappa \cdot r}{2 \cdot \pi \cdot \left(R^2 - r^2\right)} - \omega \cdot r \right) = 0 \quad (10)$$

5. Doped Vortex in a Spherical Droplet

A vortex in a spherical droplet is rectilinear at the center and is curved when it is displaced by a distance of r from the center, resembling an arc [40, 41]. In a spherical droplet, r is the distance of the vortex from the rotational axis in the equatorial plane. The curvature results from the boundary conditions of no flux through the droplet's surface. Therefore, a vortex must terminate perpendicular to the droplet surface. The calculation on the shapes, energy, angular momentum and angular velocity of a bare vortex in a droplet has been demonstrated in Refs. [31, 40, 41, 47-50]. The shape of the vortex in a spherical droplet could be obtained with good precision using a local induction approximation (LIA) [40, 41] and the condition of the stationary shape. LIA removes the singularity associated with the finite size of the vortex core. In this approximation, the contribution of the image vortex located far from the actual vortex is neglected. The values of E_{vort} and L_{vort} could then be obtained numerically from eqs. (3-4). The angular velocity, ω, is obtained as dE/dL. The results of the calculations and their fits to continuous functions are presented in the Appendix. The LIA breaks down as r approaches the droplet surface, since R-r is comparable to $2 \cdot \xi$ [41]. This range which is very close to the surface is not accessible in the case

of doped vortices due to the effect of the solvation potential. Finally, the results obtained within the LIA are very similar to those obtained previously in smaller droplets of $R_{He} < 25$ nm, by the numerically more accurate evaluation of the vortex shape in a spherical droplet based on the calculated image vortices [41]. A droplet with a vortex experience a centrifugal deformation. However, in large droplets with $R_{He} = 100$ nm the deviation of the droplet's aspect ratio from 1 is less than 1% [41] and the spherical approximation seems to be well justified. In comparison, a vortex causes much larger deformation with aspect ratio of about 1.06 in smaller droplets with $R_{He} = 5$ nm. [34, 37, 41, 51]. In addition, calculations show that even the small droplets containing several doped vortices with large separation from the center are characterized by small deviation from the spherical shape [37].

This section describes calculations done for a spherical droplet with a radius of $R_{He} = 100$ nm, with a single quantum vortex. For the sake of modelling, we assumed that the doped vortices have the same shape as the bare vortex and contain some reasonable number of Xe atoms of about 10^5 as in the recent experiments [28]. Specifically, the calculations were done with filaments containing 3.4×10^4, 1.4×10^5, 5.4×10^5 Xe atoms as in solid filaments of 100 nm length and 2.5, 5, and 10 nm radius, respectively. For comparison, He droplet with $R_{He} = 100$ nm contains $N_{He} = 8.9 \times 10^7$ atoms. Strictly, because the length of the filament depends on the distance r, according to this model, the quantity R_{Xe} should be changed with r to keep the mass at constant density of the filament. However, this effect is disregarded and the calculations at different distances r were done with the fixed mass and radius of the filament. This assumption leads to small (<20%) overestimation of the E_{vort} at large r. As a result the calculations with variable R_{Xe} are expected to be qualitatively similar. However, calculations with variable R_{Xe} are more involved as they will require calculations of vortex shape for each R_{Xe}. Most important it is not obvious that such

calculations will give any more realistic picture, as Xe filaments are solid and their shortening involves some inhomogeneous change in thickness as discussed in more details in Section 6. The calculations for the droplet use equations (7,8) with numeric dependences of $E_{vort}(r)$ and $L_{vort}(r)$ which are presented in the Appendix. For the sake of a model, we estimated the solvation potential as $100 \cdot V(r)$ where $V(r)$ is given in Fig. 1, *i.e.*, to be the same as that for the 100 nm long filament in a cylinder. The plots of equilibrium position, r, energy, E, and angular velocity, ω, of the system as a function of reduced angular momentum for bare and doped vortices are shown in Fig. 3. E, L and ω are expressed in terms of the corresponding values for a rectilinear vortex in the droplet's center with the core radius of $\xi = R_{Xe}$, for which

$$E(0) = \frac{\rho_{He} \cdot \kappa^2 \cdot R_{He}}{2 \cdot \pi} \cdot \left(\ln\left(\frac{2 \cdot R_{He}}{\xi} \right) - 1 \right) = 1.1 \times 10^4 K \qquad (11)$$

$$L(0) = \frac{2}{3} \cdot \rho_{He} \cdot \kappa \cdot R_{He} \cdot \left(R_{He}^2 - \frac{3}{2} \xi^2 \right) = 7.0 \times 10^{-4} K \cdot s \qquad (12)$$

$\omega(0) = 1.08\ 10^7$ rad s^{-1}. The numbers are for the bare rectilinear vortex in a R_{He} =100 nm droplet (ξ= 0.1 nm).

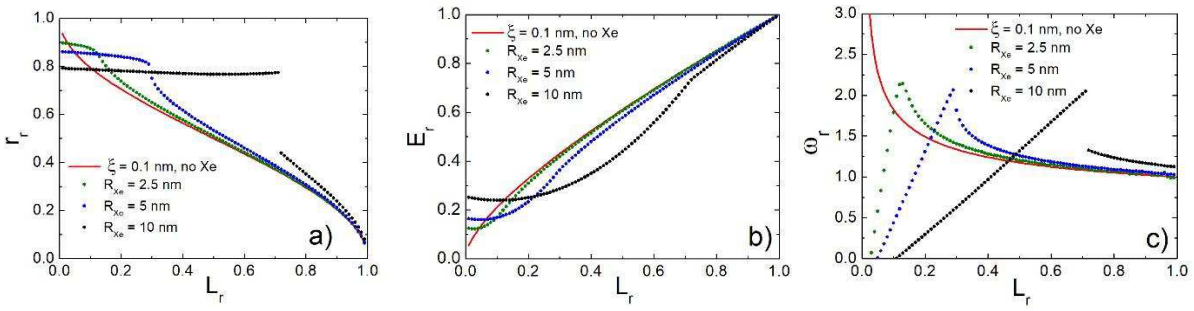

Fig. 3. Plots of (a) reduced equilibrium position r_r, (b) reduced energy E_r, and (c) reduced angular velocity ω_r as a function of reduced angular momentum L_r for a system of a curved quantum vortex in a spherical droplet with R_{He} = 100 nm. The results for a bare vortex (ξ= 0.1 nm) are shown by red curves. The results for curved vortices doped by R_{Xe}=2.5 nm, 5 nm and 10 nm filaments are shown by green, blue and black dots, respectively.

We proceed with the discussion of the results for the R_{Xe}=2.5 nm filaments. As in the case of a cylinder, the values of r_r, E_r and ω_r are similar for the doped (green curve) and bare (red curve) vortex when L_r is in the range of 1 to 0.2. However, at $L_r \approx$ 0.1-0.2, r_r changes from ~0.75 to ~0.9. At smaller L_r, r_r stays near the surface at ~0.9, which is defined by the solvation energy potential. Simultaneously, there is also an abrupt change in ω_r , and the change in slope in the E_r dependence. This behavior shows that in distinction to the doped vortex in a cylinder, where the kinematic parameters follow smooth dependences, doped vortex in a sphere experiences a bifurcation from the kinematics dominated by the vortex in the interior of the droplets to the one determined by the solvation energy potential and rotation energy of the Xe filament close to the surface. For larger R_{Xe} = 5 nm (10 nm) filaments (blue and black curves, respectively), the curves show discontinuies which appear at r_r = 0.7 (0.45) and L_r = 0.3 (0.7). Fig. 3 (c) shows that upon the jump, the angular velocity decreases approximately linearly with L_r, which is consistent with approximately constant moment of inertia of Xe close to the surface. Finally, the results in Fig. 3 show that for massive Xe filaments of R_{Xe} = 10, the kinematics is dominated by Xe and that the filament stays at large r_r ~ 0.82 at L_r <0.7.

The difference in the behavior of the doped vortex in the cylinder and in the droplet results from the different dependence of the energy and angular momentum of the vortex on the distance from the rotational axis. In a cylinder, the dependencies have a negative curvature, whereas in case of the droplet, they have a positive curvature at r_r > ~0.4. In addition, we notice that in the region of L_r close to the bifurcation the dependence of energy vs r_r has a double minimum, whereas only the values corresponding to the global minimum are reflected in Fig. 3. The occurrence of double minima may lead to some metastable configurations and delayed bifurcation vs L_r.

As already noticed, the shapes of the doped vortices may deviate from that for the bare ones. In the case of bare multiple vortices in a sphere, the vortices are expected to straighten due to the repulsive inter-vortex interaction [31, 52] [53]. Stationary configurations of a 6-vortex ring in a rotating He_{15000} droplet have been studied by DFT technique [37]. It was found that in the case of the doped vortices, the vortex cores are almost straight, whereas in an undoped droplet rotating with the same angular velocity the vortex lines would be bent. Therefore, it is of interest to compare the results in Fig. 3 with the case where the filaments are represented by straight segments parallel to the rotational axis. In reality, the shape of the doped vortices is likely somewhere in-between the curved and straight shapes, thus the corresponding solutions will delimit possible kinematics of the system. The analytic expressions for energy and angular momentum of a straight off-center vortex in a sphere have been presented in Refs. [49, 50]. The results for the straight bare and doped vortices in R_{He} = 100 nm droplet are shown in Fig. 4. As in Fig. 3, the doped vortices were approximated by cylinders of R_{Xe} = 2.5 nm, 5 nm and 10 nm containing $N_{Xe} = 3.4\times10^4$, 1.4×10^5 and 5.4×10^5, respectively.

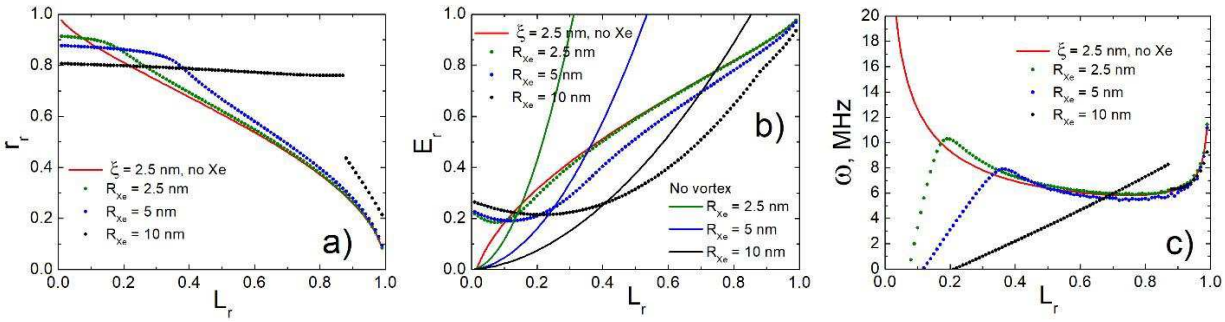

Fig. 4. Same as in Fig. 3, but for a straight bare vortex (ξ= 2.5 nm) (red) with (and straight Xe-doped vortex with R_{Xe} = 2.5 nm, 5 nm and 10 nm shown by green, blue and red dots, respectively. Continuous thin curves in b) are calculations in the absence of vortices, as described in more details in Section 6. Note that angular velocity in panel c) is expressed in absolute units.

The comparison of Fig. 3 and Fig. 4 indicates that although the results for the curved and straight vortices in a sphere differ in slight details, they show qualitatively similar behavior. In addition, the model of straight vortices [49, 50] has an analytic solution for multiple vortices and can be naturally applied for estimations of the kinematic parameters in the droplets with multiple vortices.

6. Discussion

In order to visualize vortices, the diffraction images must contain comparable x-ray scattering intensity from both the droplet and the embedded Xe atoms [27], which dictates the N_{He}:N_{Xe} ratio in the range of about 250 - 2000. The results of the model calculations shown in Figures 3 and 4 indicate that under these conditions, the positions of the doped vortices can be used for estimation of the rotational energy, angular momentum and angular velocity in the droplets. Figures 3 and 4 show that when vortices are away from the surface region with distance r less than ~$0.8 \times R_{He}$ from the center, the resulting values of E, L and ω, are close to those for a bare vortex with the core radius equal to that for the embedded Xe filament. However, when Xe clusters are found in the surface region, the system is dominated by the Xe filaments, and the kinematic parameters could not be deduced from the positions of the clusters.

In the x-ray scattering measurements, the images are taken within single ~100 fs laser pulses, which are much shorter than the typical droplet's rotational period of ~1 μs, hence no dynamics could be recorded. Accordingly, observation of a single cluster would not necessarily indicate the presence of a vortex. Therefore, it is the observation of symmetric configurations of several Xe clusters [27, 28] that indicates the presence of the quantum vortices. Xe clusters captured by the vortices are held apart by the repulsive inter-vortex interaction. The strength of the vortex-vortex repulsion can be estimated from the analytic solutions for several vortices in a

cylinder [35]. For R_{He} = 100 nm and R_{Xe} = 5 nm, the two 100 nm long vortices symmetrically displaced from the center by 50 nm (30 nm), have total kinetic energy of 5100 K (6100 K) whereas the non-additive repulsive part is 390 K (1000 K). The repulsion energy is much larger than the droplet's temperature of ~0.4 K which locks the vortices, as well as the embedded clusters, in a symmetric configuration. On the other hand, the repulsion energy is significantly smaller than the total vortex energy, so that the total energy is approximately additive for not-too-close inter-vortex distances. Note that the angular momenta of vortices are additive.

If the three-dimensional shape of the filament is known, the energy and angular momentum of the vortex could be obtained by integration from the known velocity field of a vortex or from eqs. (3, 4) if the vortex is in the plane containing the rotational axis. The energy calculation according to eq. (3) involves the determination of the value of v_S using the Biot-Savart law and shapes of the vortex and its image [40, 41]. The determination of the angular momentum from eq. (4) only requires the knowledge on the vortex shape. The diffraction at low scattering angles [27] can only yield the projection of the filaments on the detector plane. Thus, the three-dimensional image could only be implied from the flat images upon applications of certain constraints, such as that the vortex is approximately in the plane containing the rotational axis and terminates on the droplet's surface. In addition, the energy calculations require the knowledge of the width of Xe filaments, for which only an upper bound of 20 nm could be determined, [27] as limited by the current resolution. The approximation of the constant width of the filament is certainly not realistic, as filaments observed in Ref. [27] show pronounced fluctuations in linear density, which likely indicate that the filaments consist of the collection of smaller Xe clusters. Therefore, there is a rather large uncertainly in attaining the values of energy from the obtained images. In the case when the resolution is insufficient or the aspect of the images is unfortunate, such that the clusters

appear as dots [28] rather than filaments, [27] the values of E, L and ω can be estimated based on the analytic expressions for the symmetric formations of straight vortices [49, 50].

Shapes of the doped vortices in He droplets may deviate considerably from those of bare vortices. In experiments, [24, 27, 28] the droplets, which presumably already contain quantum vortices, capture large numbers of Xe atoms. Calculations indicate that single Xe atoms are bound to vortex cores by about 3-5 K [36, 54]. The embedded Xe atoms (or small Xe clusters) are captured by vortices and combine inside the vortex cores. X-ray diffraction results [27, 28] show that the shapes of the filaments vary greatly, indicating that their structure may be influenced by the reconstruction during the filament growth. The doping with Xe atoms in a typical experiment [24, 27, 28] leads to the evaporation of between 10% and 50% of the He atoms each of them carrying some unknown angular momentum. As a result, during the doping, the vortex likely moves away from the center and the initial long Xe filament must get shorter. In order to accommodate for these changes, the van der Waals bound Xe filament may fold at the surface, which causes the bulges often observed at the ends, such as in Fig. 2 of Ref. [27]. In addition, it remains unclear how close the ends of the filament approach the droplet's surface. The filaments likely stay submerged due to substantial solvation energy, and there may be some short region of near the surface, where the vortex is loose and adjusts its shape to have a perpendicular landing at the surface, such as found in recent TDDFT calculations [37].

So far, it has been assumed that a vortex is pinned to the filament over its whole length. The binding energy of a vortex to the filament can be approximated by the kinetic energy of the displaced liquid which is ~3400 K for the 100 nm long filament with R_{Xe} = 5 nm. However, the system may also undergo a transition from the state described by a doped vortex into a system described by the revolving Xe filament devoid of a vortex, while conserving the total angular

momentum, L. Fig. 4 (b) presents the calculations of E_r vs L_r for bare straight filaments of different radius, which are shown by thin continuous curves. The bare filaments occupy positions close to the droplet's surface. Fig. 4 (b) shows that at $L_r \sim 1$, the energy of the bare filament solutions exceeds that for the filament-vortex system. However, upon decrease of L_r, the bare filament solution becomes energetically favorable, with the turning point occurring at larger L_r for heavier filaments. At low L_r, the vortex may detach from the filament and annihilate at the droplet's surface. The mechanism and kinetics of the detachment remains to be elucidated. It is likely that the vortex peels off the filament starting from the loose ends close to the surface, as discussed previously in relation to cylinder-wire experiments [55]. Experimentally, the vanishing of the vortices should be evidenced by absence of the symmetric Xe formations and possibly development of the cluster-cluster conglomerates.

7. Conclusions

Recently, we have observed that Xe clusters obtained in 100 nm sized He droplets form a number of filaments arranged in symmetric configurations, [27, 28] which was assigned to pinning of Xe clusters to quantum vortices. This paper studies the effect of the mass of the filaments on the kinematics of the combined vortex-cluster system in a cylinder and in a sphere. Calculations show that the loaded vortex has larger equilibrium distance from the center as compared with a bare vortex. At small mass of the filaments, their displacement from the droplet's center can be used to obtain an estimate of the droplets rotational energy, total angular momentum and angular velocity, which are close to the corresponding values in the bare vortex. However, at large mass of the filament and small values of the total angular momentum, the filament-vortex system is dominated by the motion of the filament. In such conditions, the system occupies the surface region, where its position is mostly defined by the balance of the solvation energy of the filament

in liquid helium and its rotation energy. Calculations also reveal that upon decrease of the total angular momentum beyond a certain value, the energy of the vortex-filament system becomes larger than that for a bare filament, upon which the vortex may detach and annihilate on the droplet's surface.

Acknowledgements

This work was supported by the NSF Grants DMR-1501276 and DMR-1701077. The authors are thankful to Dr. Curtis Jones for his early contributions to this work and to Sean O'Connell, Rico Mayro Tanyag and Deepak Verma, for careful reading of the manuscript.

Appendix

In order to calculate E_{vort}, L_{vort}, and $\omega = dE/dL$, of a bare curved vortex with different core size in spherical He droplets, equations (3) and (4) are used. Numeric calculations of the angular momentum via eq. (3) is straightforward. On the other hand, the energy calculation takes a much longer time. To expedite the calculations, a summation method can be utilized by dividing a certain two-dimensional area of the integration, close to the vortex into smaller discrete areas. However, even then the values of energy show some noise, since the smaller discrete areas of integration are still much larger than the required infinitesimal areas of integration. On the other hand, we found that, the results of the LIA calculations of the E_{vort} and L_{vort} versus r/R for a bare vortex could be well-fitted by a function

$$f\left(\frac{r}{R}\right) = 1 - a + a \cdot \cos\left(\frac{\pi \cdot \frac{r}{R}}{b}\right). \qquad \text{(A1)}$$

The parameters a and b have been obtained from a limited number of high accuracy calculations of E_{vort} and L_{vort} at different displacement for 0.1 nm, 2.5, 5 and 10 nm. Table A1 gives the obtained parameters. The resulting fitted dependencies are presented in Fig. A1 and were used to obtain the continuous outcome curves presented in Fig. 3. In Fig. A1, the E_{vort} and L_{vort} are expressed in units of the corresponding values for central rectilinear vortex with the core radius of ξ, which are given by eqs (11,12). It is seen that the reduced values of energy, angular momentum and angular velocity for bare vortices with different core sizes are very similar.

Table A1. Parameters a and b in eq.(A1) used to fit E_{vort} and L_{vort} vs r/R.

Vortex core radius, ξ, nm	E_{vort} fit		L_{vort} fit	
	a	b	a	b
0.1	0.563	1.278	0.500	1
2.5	0.545	1.227	0.502	1
5.0	0.533	1.190	0.504	1
10.0	0.521	1.149	0.505	1

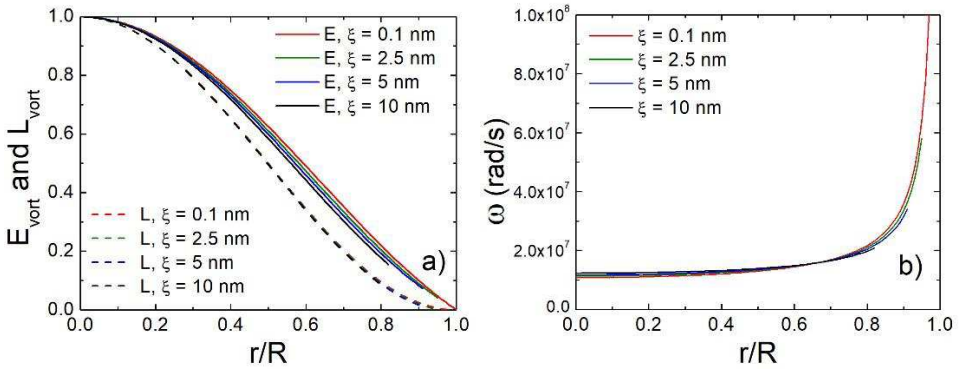

Fig. A1. Reduced energy, reduced angular momentum in panel (a) and angular velocity in panel (b) of a bare vortex with core radius of ξ = 0.1, 2.5, 5 and 10 nm versus the reduced displacement from the droplet's center in the droplet having R = 100 nm.

References

[1] R.J. Donnelly, Quantized Vortices in Helium II, Cambridge University Press, Cambridge, 1991.
[2] R.P. Feynman, Application of quantum mechanics to liquid helium, in: C.J. Gorter (Ed.), Progress in Low Temperature Physics, North-Holland Publishing Company, Amsterdam, 1955, pp. 1.
[3] L. Pitaevskii, S. Stringari, Bose-Einstein Condensation and Superfluididty, Oxford University Press, Oxford, 2016.
[4] A.L. Fetter, Rotating trapped Bose-Einstein condensates, Rev. Mod. Phys. 81, 647 (2009).
[5] M.R. Matthews, B.P. Anderson, P.C. Haljan, D.S. Hall, C.E. Wieman, E.A. Cornell, Vortices in a Bose-Einstein condensate, Phys. Rev. Lett. 83, 2498 (1999).
[6] K.W. Madison, F. Chevy, W. Wohlleben, J. Dalibard, Vortex formation in a stirred Bose-Einstein condensate, Phys. Rev. Lett. 84, 806 (2000).
[7] J.R. Abo-Shaeer, C. Raman, J.M. Vogels, W. Ketterle, Observation of vortex lattices in Bose-Einstein condensates, Science 292, 476 (2001).
[8] G.A. Williams, R.E. Packard, Photographs of Quantized Vortex Lines in Rotating He II, Phys. Rev. Lett. 33, 280 (1974).
[9] E.J. Yarmchuk, M.J.V. Gordon, R.E. Packard, Observation of Stationary Vortex Arrays in Rotating Superfluid-Helium, Phys. Rev. Lett. 43, 214 (1979).
[10] E.J. Yarmchuk, R.E. Packard, Photographic Studies of Quantized Vortex Lines, J. Low Temp. Phys. 46, 479 (1982).
[11] W. Guo, M. La Mantia, D.P. Lathrop, S.W. Van Sciver, Visualization of two-fluid flows of superfluid helium-4, Proc. Natl. Acad. Sci. USA 111, 4653 (2014).
[12] D.P. Meichle, C. Rorai, M.E. Fisher, D.P. Lathrop, Quantized vortex reconnection: Fixed points and initial conditions, Phys. Rev. B 86, 014509 (2012).
[13] G.P. Bewley, D.P. Lathrop, K.R. Sreenivasan, Superfluid helium - Visualization of quantized vortices, Nature 441, 588 (2006).
[14] E. Fonda, D.P. Meichle, N.T. Ouellette, S. Hormoz, D.P. Lathrop, Direct observation of Kelvin waves excited by quantized vortex reconnection, Proc. Natl. Acad. Sci. USA 111, 4707 (2014).
[15] D.E. Zmeev, F. Pakpour, P.M. Walmsley, A.I. Golov, W. Guo, D.N. McKinsey, G.G. Ihas, P.V.E. McClintock, S.N. Fisher, W.F. Vinen, Excimers He_2* as Tracers of Quantum Turbulence in He-4 in the T=0 Limit, Phys. Rev. Lett. 110, 175303 (2013).
[16] W. Guo, D.N. McKinsey, A. Marakov, K.J. Thompson, G.G. Ihas, W.F. Vinen, Visualization Technique for Determining the Structure Functions of Normal-Fluid Turbulence in Superfluid Helium-4, J. Low Temp. Phys. 171, 497 (2013).
[17] W. Guo, S.B. Cahn, J.A. Nikkel, W.F. Vinen, D.N. McKinsey, Visualization Study of Counterflow in Superfluid He-4 using Metastable Helium Molecules, Phys. Rev. Lett. 105, 045301 (2010).
[18] M.A. Weilert, D.L. Whitaker, H.J. Maris, G.M. Seidel, Magnetic levitation of liquid helium, J. Low Temp. Phys. 106, 101 (1997).
[19] M.A. Weilert, D.L. Whitaker, H.J. Maris, G.M. Seidel, Magnetic levitation and noncoalescence of liquid helium, Phys. Rev. Lett. 77, 4840 (1996).
[20] U. Henne, J.P. Toennies, Electron Capture by Large Helium Droplets, J. Chem. Phys. 108, 9327 (1998).
[21] R.E. Grisenti, J.P. Toennies, Cryogenic Microjet Source for Orthotropic Beams of Ultralarge Superfluid Helium Droplets, Phys. Rev. Lett. 90, 234501 (2003).
[22] M. Kühnel, N. Petridis, D.F.A. Winters, U. Popp, R. Dörner, T. Stöhlker, R.E. Grisenti, Low-Z internal target from a cryogenically cooled liquid microjet source, Nucl Instrum Meth A 602, 311 (2009).
[23] L.F. Gomez, E. Loginov, R. Sliter, A.F. Vilesov, Sizes of large helium droplets, J. Chem. Phys. 135, 154201 (2011).

[24] L.F. Gomez, K.R. Ferguson, J.P. Cryan, C. Bacellar, R.M.P. Tanyag, C. Jones, S. Schorb, D. Anielski, A. Belkacem, C. Bernando, R. Boll, J. Bozek, S. Carron, G. Chen, T. Delmas, L. Englert, S.W. Epp, B. Erk, L. Foucar, R. Hartmann, A. Hexemer, M. Huth, J. Kwok, S.R. Leone, J.H.S. Ma, F.R.N.C. Maia, E. Malmerberg, S. Marchesini, D.M. Neumark, B. Poon, J. Prell, D. Rolles, B. Rudek, A. Rudenko, M. Seifrid, K.R. Siefermann, F.P. Sturm, M. Swiggers, J. Ullrich, F. Weise, P. Zwart, C. Bostedt, O. Gessner, A.F. Vilesov, Shapes and vorticities of superfluid helium nanodroplets, Science 345, 906 (2014).
[25] L.F. Gomez, E. Loginov, A.F. Vilesov, Traces of vortices in superfluid helium droplets, Phys. Rev. Lett. 108, 155302 (2012).
[26] R.M. Tanyag, C.F. Jones, C. Bernando, S.M.O. O'Connell, D. Verma, A.F. Vilesov, Experiments with Large Superfluid Helium Nanodroplets, in: A. Osterwalder, O. Dulieu (Eds.), Cold Chemistry: Molecular Scattering and Reactivity Near Absolute Zero, Royal Society of Chemistry, Cambridge, 2017, pp. 389.
[27] R.M.P. Tanyag, C. Bernando, C.F. Jones, C. Bacellar, K.R. Ferguson, D. Anielski, R. Boll, S. Carron, J.P. Cryan, L. Englert, S. Epp, B. Erk, L. Foucar, L.F. Gomez, R. Hartmann, D.M. Neumark, D. Rolles, B. Rudek, K.R. Siefermann, J. Ullrich, F. Weise, C. Bostedt, O. Gessner, A.F. Vilesov, X-ray coherent diffraction imaging by immersion in nanodroplets, Struct. Dynam. 2, 051102 (2015).
[28] C.F. Jones, C. Bernando, R.M.P. Tanyag, C. Bacellar, K.R. Ferguson, L.F. Gomez, D. Anielski, A. Belkacem, R. Boll, J. Bozek, S. Carron, J.P. Cryan, L. Englert, S.W. Epp, B. Erk, L. Foucar, R. Hartmann, D.M. Neumark, D. Rolles, A. Rudenko, K.R. Siefermann, F. Weise, B. Rudek, F.P. Sturm, J. Ullrich, C. Bostedt, O. Gessner, A.F. Vilesov, Coupled motion of Xe clusters and quantum vortices in He nanodroplets Phys. Rev. B. 93, 180510(R) (2016).
[29] P.K. Newton, G. Chamoun, Vortex Lattice Theory: A Particle Interaction Perspective, Siam Rev 51, 501 (2009).
[30] K.W. Schwarz, 3-Dimensional Vortex Dynamics in Superfluid He-4 - Line-Line and Line-Boundary Interactions, Phys. Rev. B 31, 5782 (1985).
[31] R. Hanninen, A.W. Baggaley, Vortex filament method as a tool for computational visualization of quantum turbulence, Proc. Natl. Acad. Sci. USA 111, 4667 (2014).
[32] H. Adachi, S. Fujiyama, M. Tsubota, Steady-state counterflow quantum turbulence: Simulation of vortex filaments using the full Biot-Savart law, Phys. Rev. B 81, 104511 (2010).
[33] S. Yui, M. Tsubota, Counterflow quantum turbulence of He-II in a square channel: Numerical analysis with nonuniform flows of the normal fluid, Phys. Rev. B 91, 184504 (2015).
[34] F. Ancilotto, M. Pi, M. Barranco, Vortex arrays in nanoscopic superfluid helium droplets, Phys. Rev. B 91, 100503(R) (2015).
[35] G.B. Hess, Angular Momentum of Superfluid Helium in a Rotating Cylinder, Phys. Rev. 161, 189 (1967).
[36] F. Ancilotto, M. Pi, M. Barranco, Vortex arrays in a rotating superfluid ^{4}He nanocylinder, Phys. Rev. B 90, 174512 (2014).
[37] F. Coppens, F. Ancilotto, M. Barranco, N. Halberstadt, M. Pi, Capture of Xe and Ar atoms by quantized vortices in He-4 nanodroplets, Phys. Chem. Chem. Phys. 19, 24805 (2017).
[38] I.A. Pshenichnyuk, N.G. Berloff, Inelastic scattering of xenon atoms by quantized vortices in superfluids, Phys. Rev. B 94, 184505 (2016).
[39] I.A. Pshenichnyuk, Static and dynamic properties of heavily doped quantum vortices, New Journal of Physics 19, 105007 (2017).
[40] G.H. Bauer, R.J. Donnelly, W.F. Vinen, Vortex Configurations in a Freely Rotating Superfluid Drop, J. Low Temp. Phys. 98, 47 (1995).
[41] K.K. Lehmann, R. Schmied, Energetics and possible formation and decay mechanisms of vortices in helium nanodroplets, Phys. Rev. B 68, 224520 (2003).
[42] L. Pitaevskii, S. Stringari, Superfluid Effects in Rotating Helium Clusters, Z. Phys. D 16, 299 (1990).
[43] Y.K. Kwon, K.B. Whaley, Atomic-scale quantum solvation structure in superfluid helium-4 clusters, Phys. Rev. Lett. 83, 4108 (1999).

[44] M. Barranco, R. Guardiola, E.S. Hernandez, R. Mayol, J. Navarro, M. Pi, Helium nanodroplets: an overview, J. Low Temp. Phys. 142, 1 (2006).
[45] K.K. Lehmann, Potential of a neutral impurity in a large He-4 cluster, Mol. Phys. 97, 645 (1999).
[46] A.A. Radzig, B.M. Smirnov, Reference data on atoms, molecules, and ions, Springer-Verlag, Berlin, Heidelberg, New York, Tokyo, 1985.
[47] D. Kivotides, C.F. Barenghi, Y.A. Sergeev, Interactions between particles and quantized vortices in superfluid helium, Phys. Rev. B 77, 014527 (2008).
[48] D. Kivotides, Y.A. Sergeev, C.F. Barenghi, Dynamics of solid particles in a tangle of superfluid vortices at low temperatures, Phys Fluids 20, 055105 (2008).
[49] S.T. Nam, Comparison between the vortex patterns in superfluid helium in rotating cylindrical and spherical vessels, J Korean Phys Soc 35, 416 (1999).
[50] S.T. Nam, G.H. Bauer, R.J. Donnelly, Vortex patterns in a freely rotating superfluid, J Korean Phys Soc 29, 755 (1996).
[51] F. Ancilotto, M. Barranco, F. Coppens, J. Eloranta, N. Halberstadt, A. Hernando, D. Mateo, M. Pi, Density functional theory of doped superfluid liquid helium and nanodroplets, Int. Rev. Phys. Chem. 36, 621 (2017).
[52] V.B. Eltsov, R. de Graaf, P.J. Heikkinen, J.J. Hosio, R. Hanninen, M. Krusius, Vortex Formation and Annihilation in Rotating Superfluid He-3-B at Low Temperatures, J. Low Temp. Phys. 161, 474 (2010).
[53] V.B. Eltsov, R. de Graaf, P.J. Heikkinen, J.J. Hosio, R. Hanninen, M. Krusius, V.S. L'vov, Stability and Dissipation of Laminar Vortex Flow in Superfluid He-3-B, Phys. Rev. Lett. 105, 125301 (2010).
[54] F. Dalfovo, R. Mayol, M. Pi, M. Barranco, Pinning of quantized vortices in helium drops by dopant atoms and molecules, Phys. Rev. Lett. 85, 1028 (2000).
[55] W.F. Vinen, Detection of Single Quanta of Circulation in Liquid Helium II, Proc R Soc Lon Ser-A 260, 218 (1961).